Beyond Graphene: Stable Elemental Monolayers of Silicene and Germanene

Nathanael J. Roome*,[†] and J. David Carey*,[†,‡]

[†]Advanced Technology Institute, University of Surrey, Guildford GU2 7XH, United Kingdom
[‡]Department of Electronic Engineering, University of Surrey, Guildford GU2 7XH, United Kingdom

S *Supporting Information*

ABSTRACT: Two-dimensional materials are one of the most active areas of nanomaterials research. Here we report the structural stability, electronic and vibrational properties of different monolayer configurations of the group IV elemental materials silicene and germanene. The structure of the stable configuration is calculated and for planar and low (<1 Å) atomic buckling configurations, analysis of the electronic band structure reveals linear band dispersion giving rise to massless Dirac Fermions with a Fermi velocity about two-thirds that of graphene. Monolayer stability is shown to be directly attributed to the phonons present with the instability being driven by the out-of-plane ZA and ZO phonon modes. Long momentum relaxation lengths and high carrier mobilities are predicted for silicene and germanene based devices as carrier relaxation via phonon scattering is found to be inhibited as the electron−optical phonon coupling matrix elements are calculated to be small, being about a factor of 25 times smaller than in graphene. The consequences for phonon scattering, high energy electrical transport and integration of elemental monolayers into electronic devices are further discussed.

KEYWORDS: *2D monolayers, silicene, germanene, graphene, electron−phonon coupling, carrier relaxation*
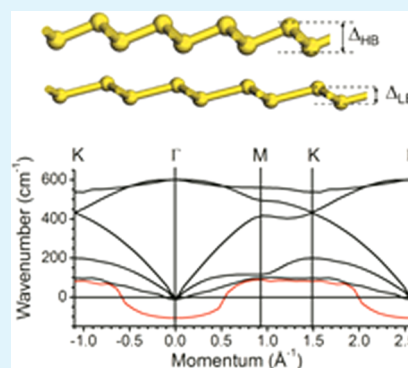
1. INTRODUCTION

Two-dimensional (2D) layered van der Waals materials[1] such as graphene,[2] hexagonal boron nitride[3] and the transition metal dichalcogenides[4] offer considerable potential to exploit a range of attractive electronic properties and to take advantage of their inherent 2D structure, either as single or few layers, or as part of a layered heterostructure.[1−4] Graphene is the most widely studied 2D monolayer (ML) material and many of its properties reflect its distinctive low energy electronic band structure.[5] Around the Dirac point, where the occupied π and unoccupied π^* states cross, the band dispersion is linear leading to quasiparticles that mimic the characteristics of massless Dirac Fermions. This results in carriers that propagate with a Fermi velocity, v_F, that is about 1/300th of the speed of light, leading to high room-temperature mobilities. Graphene has already demonstrated these properties serving variously as a calibration for universal constants,[6] as a transparent contact in solar cells[7] and in high frequency electronics with high cutoff frequencies.[8] Although there is sustained research effort in the study of graphene, recent attention has turned to alternative 2D materials. Of particular interest are the other group IV elemental materials silicene and germanene as predominately sp[2] near-planar analogues of Si and Ge, respectively. These materials possess a (near) honeycomb lattice and a general feature of a 2D honeycomb lattice of identical atoms is the emergence of linear band dispersion behavior around the Fermi energy at the K point and the appearance of massless Dirac Fermions, which can lead to high carrier mobility.

To date, silicene has been produced on Ag(111) substrates[9,10] and Ir(111) substrates,[11] on Ag(110) as nano-ribbons[12] and recently on the conductive ceramic ZrB$_2$ (0001)/ Si(111).[13] An energy gap between the occupied and unoccupied electron states can be engineered in these monolayers through exposure to hydrogen. For example Restrepo et al. have shown that complete hydrogenation of silicene produces silicane, which has an indirect energy gap of 2.94 eV.[14] However, for a 1.6% tensile strain, the band gap changes to be direct and there is an 18-fold increase in electron mobility to be in excess of 8550 cm^2/(V s). A hydrogenated form of germanene, germanane, has also recently been exfoliated[15] and it has been proposed that stable germanene may be able to be grown on GaAs,[16] though confirmation of the growth of germanene on metal substrates is awaited. Ab initio calculations have also recently investigated the properties of stanene, a monolayer version of sp[2] tin, and found that it may be a quantum spin Hall insulator with a direct energy gap of 0.3 eV.[17] Given silicon's pre-eminence as an electronic material, and the possibility of easier incorporation of silicene in devices compared to graphene, knowledge of the electronic and vibrational properties of its 2D analogue, and related materials, is of both fundamental and applied interest.

Previous ab initio studies[18] have demonstrated that both silicene and germanene can adopt two different buckled geometries, referred to as low buckling (LB, less than 1 Å) and high buckling (HB). In both cases, atoms in different triangular sublattices are offset from planarity by a total buckling height, Δ, (Figure 1a). Experimental evidence of buckling has been obtained by scanning tunnelling microscopy measurements,[9−12] the extent of which depends on the substrate used. Key questions that are therefore to be addressed in the present study include the quantification of the buckling for freestanding MLs, its effect on the electronic band structure
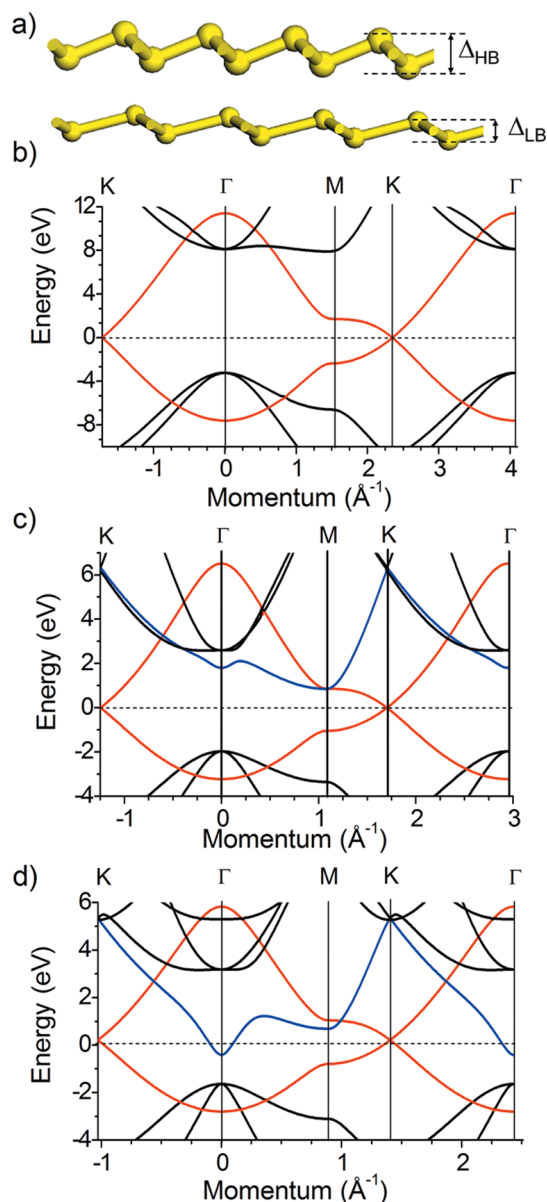
Figure 1. (a) Atomic configuration in nonplanar geometry with the atom buckling characterized by total height Δ; each sublattice is offset from planarity by a height $\Delta/2$. HB and LB refer to high and low buckling, respectively. The electronic band structure for free-standing planar monolayers of (b) graphene, (c) silicene and (d) germanene; the occupied π and unoccupied π^* bands are indicated by red lines. The unoccupied "stray" band, referred to in the text, is indicated by the blue line in panels b and c; this band appears at much higher energies in graphene.

and phonon dispersion, and the identification of important phonon modes, including Raman active modes. This knowledge will allow us to identify the factors that affect ML stability and further allow us to calculate the electron−phonon coupling (EPC) matrix elements. The interaction between carriers and phonons is one of the most important in condensed matter physics and it plays an important role in electrical transport, where phonon absorption and optical phonon emission at high electric fields strongly affects mobility and thermal transport.[19]

Carrier relaxation in the presence of an electric field is usually described by assuming nonrelativistic electron propagation, where the phonons are treated adiabatically within the Born−Oppenheimer approximation (BOA) as frozen displacements of the electronic ground state. In graphene, the inverse of the zone center optical phonon frequency, which plays an important role in hot carrier relaxation, is much smaller than the electron momentum relaxation time, τ_R, leading to a breakdown of this approximation.[20] Near the Dirac point in silicene, τ_R has been calculated[21] to be as long as 1.8 ps; therefore, analysis of the vibrational properties will also determine whether the BOA can be applied to adiabatic carrier relaxation in silicene and germanene. In this study, we explore, using ab initio methods, the properties and stability of group IV 2D layered materials. Comparison of silicene and germanene's properties, such as Fermi velocity, band structure and phonon dispersion with graphene will provide new insight into the structural, electronic and vibrational properties of elemental monolayers beyond graphene and their potential insight into their electronic applications.

2. COMPUTATIONAL DETAILS

The optimized (planar and buckled) atomic arrangements, electronic band structure and phonon dispersion curves are calculated from density functional theory (DFT) and density functional perturbation theory (DFPT) via diagonalization of the dynamical matrix, respectively. A revised Perdew−Burke−Ernzerhof functional[22] within the generalized gradient approximation using DMol[3] (reference 23) and CASTEP codes[24] is used. Free-standing MLs are described by their crystallographic space group, $P6/mmm$ (planar) and $P−3m1$ (buckled configurations), with layers separated by a vacuum slab of greater than 10 Å in thickness. Initially, the atoms undergo a geometric optimization by forcing the system into an atomic arrangement that is subsequently allowed to relax into the minimum energy state where the forces on the atoms are less than 0.01 eV/Å. The Brillouin zone undergoes an energy optimization with a sampling Monkhorst−Pack grid chosen to achieve a K point separation <0.025 Å^{-1} (better than 12 × 12 × 2). Plane wave cutoff energies within CASTEP are set above 400 eV. Phonon dispersion curves are calculated using both the finite displacement method[24] and the linear response method.[25] Both methods rely on atomic perturbations of the atom geometry followed by a relaxation to define the vibrational mode. The finite displacement method produces smooth phonon branches and accurate calculations of vibrational frequencies but can miss kinks or sharp changes. The linear response method captures the finer detail of higher energy vibrational modes but can produce errors across the branches. When EPC matrix elements are calculated, it is necessary to examine for kinks in the phonon branches as these are signatures of the presence of Kohn anomalies. Such features are associated with the softening of the vibrational frequencies for phonons that connect states near the Fermi surface; hence a combination of the simulation methods is employed. In hexagonal lattices, Kohn anomalies may rise at the zone center, associated with the double degenerate E_{2g} phonon mode, or at the zone boundary, associated with the A_1' phonon mode. The appearance of negative phonon frequencies in the output of the phonon dispersion calculations is a sign of monolayer instability.

Table 1. Calculated Properties for Graphene, Silicene and Germanene in the Planar, Low and High Buckling Forms[a]

atomic mass	zone point	graphene 12.01	silicene 28.09			germanene 72.64		
		planar	planar	low buckling	high buckling	planar	low buckling	high buckling
lattice constant, (Å)		2.43	3.85	3.88	2.71	4.07	4.06	2.97
buckling height, Δ (Å)				0.44	2.15		0.67	2.28
energy stability (eV/atom)			0.62	0.45	0.61	0.54	0.28	0.38
Fermi velocity, v_F ($\times 10^5$ m/s)		8.0	5.21	5.27		5.59	5.09	
highest frequency vibration, ω (cm^{-1})	Γ	1566	604	556	392	336	292	195
	L	1377	475	503	216	307	274	106
D^2, (eV/Å)^2	Γ	42.6	1.4	1.9		0.3	1.6	
	K	65.0	2.9	2.7		2.4	1.4	
g^2, (eV^2)	Γ	0.038	0.001	0.002		0.0002	0.001	
	K	0.076	0.004	0.003		0.002	0.001	
predicted monolayer stability		stable	unstable	stable	unstable	unstable	stable	unstable

[a]The parameters are lattice constant, total atomic buckling (Δ), energy stability of the atoms relative to bulk crystal, Fermi velocity, highest phonon frequencies at the high symmetry Γ and K points and electron−phonon coupling matrix elements. The free-standing material stability is predicted based on analysis of these properties.

3. RESULTS AND DISCUSSION: PLANAR MONOLAYERS OF GRAPHENE, SILICENE AND GERMANENE

Figure 1b−d shows the electronic band structure for graphene, planar silicene and germanene, where linear band dispersion behavior around the Dirac point at the K point in the Brillouin zone, is seen. The π and π^* bands in all three materials (red lines in Figure 1) are associated with the out-of-plane p_z molecular orbitals; there are also several σ and σ^* bands associated with in-plane sp^2 bonding and antibonding orbitals. In Figure 1c,d, the π and π^* bands in the planar silicene and germanene (red lines) are still observed though the energy separation at the Γ point is lower due to the weaker π bonding associated with the larger lattice constant. From the slope of the band dispersion around the Dirac point, the Fermi velocity is calculated to be 8.0×10^5 m/s in graphene, but is lower in planar silicene and germanene, 5.2×10^5 and 5.6×10^5 m/s, respectively, (Table 1). The hopping integral, t, associated with electron hopping between triangular sublattices, is calculated from v_F via $t = (2\hbar v_F)/(\sqrt{3}a)$, where a is the lattice constant; the values of t are calculated to be 2.50, 1.03 and 1.05 eV, respectively. The reduction in t found in silicene and germanene, when compared to graphene, is also associated with weaker π bonding. The high value of v_F and the linear band dispersion leading to massless Dirac Fermions will lead to high carrier mobilities in silicene and germanene (provided that the coupling to phonons is weak, as discussed later).

In planar germanene, the electronic band structure shows a band (Figure 1d, blue line) crossing the Fermi level around the Γ point, which results in a finite density of states and quasi-metallic behavior. There is also an upward shift of 0.35 eV of the Dirac point relative to the Fermi level. The origin of this "stray" band is the subject of some debate having previously[26] been assigned to a π^* antibonding band, where it was proposed that in-plane compression pushed this band into the valence band but preserved the cone-like shape of the π and π^* bands. We propose this assignment to be incorrect, rather we propose that the band is associated with an σ^* antibonding band. Orbital analysis of all the bands crossing the Γ point in all three materials has been performed, see Tables S1−S3 in the Supporting Information, where it shows that the stray band in

germanene has σ^* character. Such analysis consists of identifying a σ wave function as one where the orbital phase does not change upon a horizontal reflection in the plane containing the bond; whereas π states are characterized by a change of phase upon 180° rotation along the direction of the bond. The occupancy of this antibonding orbital contributes to the instability of planar germanene. The stability of the planar MLs can be further inferred from analysis of the phonon dispersion curves, Figure 2. In graphene, the phonon branches at the Γ point are, in order of decreasing frequency, the doubly degenerate longitudinal optical (LO) and transverse optical (TO) modes at 1566 cm^{-1}, the out-of-plane optical (ZO) mode (877 cm^{-1}) and three transverse, longitudinal and out-of-plane acoustic (TA, LA, ZA) modes. At the K point, the modes present are the TO mode (1337 cm^{-1}), doubly degenerate LO and LA modes (1204 cm^{-1}), TA mode (983 cm^{-1}) and the degenerate ZO and ZA modes (532 cm^{-1}).

Within the D$_{6h}$ point symmetry of the planar MLs, the E$_{2g}$ LO mode at the Γ point, and the A$_1'$ TO mode at the K point correspond to the Raman G and defect-activated D peaks, respectively. The corresponding modes in silicene and germanene are given in Table 1, and our calculations predict that for free-standing undoped monolayers, respectively, a Raman peak associated with the E$_{2g}$ mode of vibration at around 604 cm^{-1} (silicene) and 336 cm^{-1} (germanene), analogous to the G band along with a defect-activated D peak at 475 cm^{-1} (silicene) and 307 cm^{-1} (germanene). Substantial negative frequencies are observed in the calculated phonon dispersion of silicene and germanene (Figure 2b,c); the exact vibrational mode connected with a particular branch being resolved at the high symmetry Γ and K points. For planar silicene, negative vibrations are associated with the ZO mode around the Γ point; this out-of-plane vibration causes atomic buckling to increase, resulting in the low buckling configuration.

We propose that if the amplitude of this ZO mode vibration can be suppressed, equivalent to removing the zero point vibrational energy contribution to the overall ML stabilization energy, e.g., by the selection of an appropriate substrate, which would dampen the out-of-plane vibrational mode, then planar silicene could be produced. However, for germanene, the absence of any positive frequencies associated with the ZO
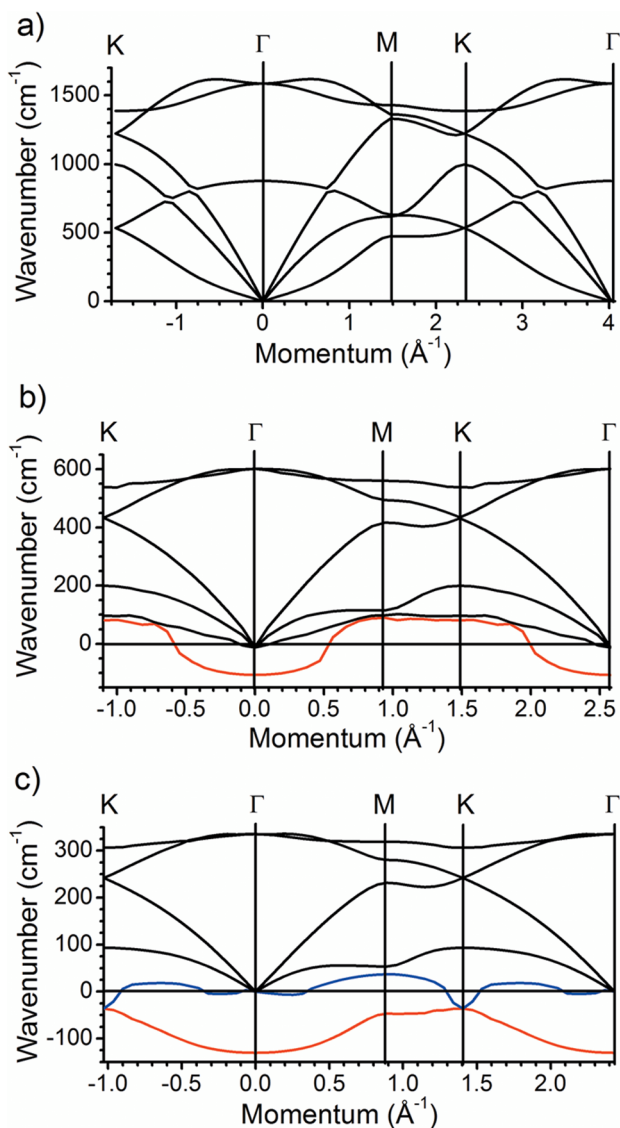
Figure 2. Phonon dispersion curves for (a) graphene, (b) planar silicene and (c) planar germanene monolayers. Negative values of phonon frequencies can be used to infer the stability of the monolayer. The ZO phonon mode is marked in red in panels b and c showing the extent of the negative frequencies. The ZA phonon mode in germanene is marked in blue in panel c.

mode, and the negative frequencies with the ZA mode, results in two vibrational modes contributing to ML structural instability. Given the extent of the negative frequencies present associated with the two modes, stable planar free-standing germanene is unlikely.

4. RESULTS AND DISCUSSION: BUCKLED MONOLAYERS OF SILICENE AND GERMANENE

Turning to the buckled configurations, Figure 3, shows the electronic band structures for silicene and germanene in both LB and HB configurations. The minimum energy low bucking configuration in silicene (germanene) is characterized by $\Delta_{LB} =$ 0.44 Å (0.67 Å), whereas in the high buckling configuration $\Delta_{HB} = 2.15$ Å (2.28 Å), respectively. Table 1 shows that in terms of relative stability (calculated relative to bulk Si or Ge), the LB form of silicene is 0.17 eV/atom more stable than the planar form, which itself is comparable in energy to the HB

form. In the case of germanene, the LB form is again the most stable, being 0.26 eV/atom more stable than the energy of the planar form though, in this case, the HB form of Ge is much closer in energy to the LB form being only 0.1 eV/atom higher in energy. These stabilization energies are larger than those calculated by Scalise et al., who calculate, using either the local density approximation or the generalized gradient approximation, stabilization energies of silicene of 14 to 27 meV/atom, respectively.[27] From Figure 3, in the LB configuration, a low energy linear dispersion behavior is seen around the K point with a Fermi velocity of 5.3×10^5 m/s in silicene and 5.1×10^5 m/s in germanene; similar to the values found in the planar MLs. A 0.6×10^5 m/s decrease in the Fermi velocity from planar to LB germanene is attributed to the increased distance between the nearest neighbor atoms from 2.351 to 2.439 Å.

Lower values of Fermi velocity were found in the study by Guzmán-Verri and Lew Yan Voon who explored using a first nearest neighbor and second nearest neighbor tight-binding formulism in calculating the band structure.[28] They found in their planar form of silicene a Fermi velocity of about 10^5 m/s, about half that found in this study, but that in a buckled form the Fermi velocity had reduced to 10^4 m/s. In that study, the atomic buckling is characterized by half of the Si atoms being vertically displaced from the Si(111) plane by an amount that is approximately equal to 1.1 Å, intermediate between the low and high buckling found in this ab initio study. In both buckled germanene configurations, the stray σ^* band seen crossing the Fermi level in planar germanene is no longer present. Figure 3 also shows the low energy σ and σ^* bands positions in LB silicene and germanene near the Γ point are getting progressively closer together as a consequence of the buckled geometry. In graphene, the sp^2 states are constructed from s, p_x and p_y carbon orbitals, leading to σ state formation; in a fully sp^3 material, such as diamond, the states are constructed from a combination of s, p_x, p_y and p_z states. External methods such as thermal annealing or ion implantation[29] can respectively change the globally or locally sp^3 to sp^2 fraction in mixed-phased materials. The p_z orbitals in graphene go on to form the π states the π and σ states are decoupled from one other. Coupling and admixture to introduce some sp^3 character occurs in silicene and germanene as the π bonding is weaker, as the bond length is longer, resulting in the loss of planarity. As the atoms in the layer are offset from the atomic plane, the usually perpendicular p_z orbital is increasingly interacting with the sp^2 orbitals due to the reduced angle between them. This additional interaction contributes to the bonding and results in a mixed-phase material that is predominantly sp^2 with a small amount of sp^3 character present. The buckling also lowers several point group symmetries (D_{6h} to D_{3d}) and this in turn breaks several energy degeneracies associated with the bands. In the electronic band structure, this is characterized by the emergence of anticrossing bands. The effects are most prominent in germanene, as the buckling (0.67 Å) is 50% greater than that of silicene (0.44 Å).

Previous STM measurements[11] of silicene grown on Ir(111) have revealed a $\sqrt{3} \times \sqrt{3}$ low buckled (0.6 Å) silicene construction on a $\sqrt{7} \times \sqrt{7}$ Ir(111) superstructure. The periodicity of the silicene layer on Ir(111) was found to be about 7.2 Å, which is larger than 6.6 Å; which is $\sqrt{3} \times$ lattice constant for low buckled silicene calculated here. The longer lattice constant, and hence longer Si–Si bond, may indicate stabilization through charge transfer from the Ir substrate via p–d orbital hybridization. Cinquanta et al., in their STM studies of silicene on Ag(111), reported a 4×4 and a $\sqrt{13} \times$
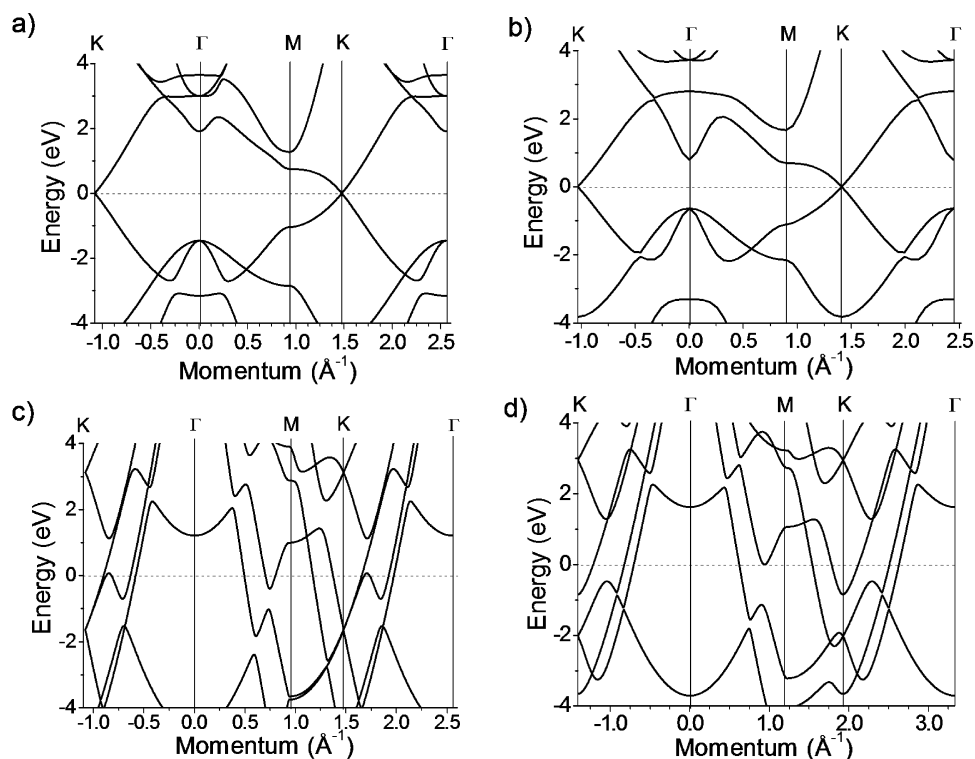
Figure 3. Electronic band structure of (a) LB silicene, (b) LB germanene, (c) HB silicene and (d) HB germanene. Linear dispersion at the K point is observed in the low buckling configurations but is absent in the high buckling configuration.
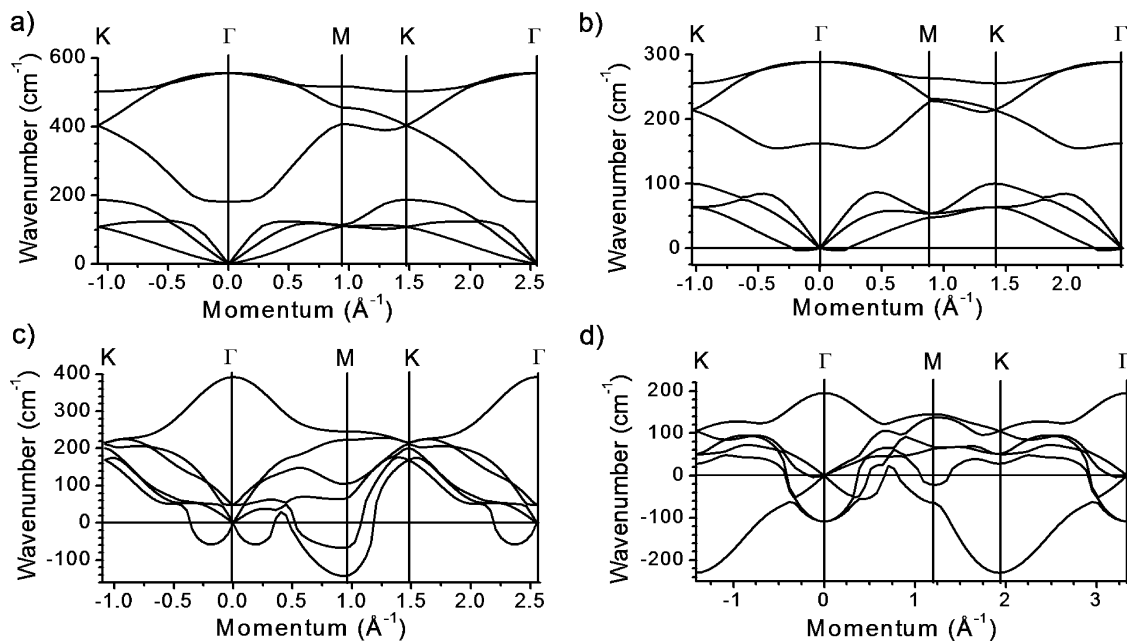
Figure 4. Phonon dispersion curves for (a) LB silicene, (b) LB germanene, (c) HB silicene and (d) HB germanene. The absence of significant negative frequencies for the low buckling cases would suggest they are stable. In the high buckling forms there are substantial LO and TO branches calculated to have negative frequencies, indication that these configurations are unstable.

$\sqrt{13}$ superstructure as the two most common atomic arrangements grown at the lower growth temperature of 250 °C; above a growth temperature of 270 °C, a $2\sqrt{3} \times 2\sqrt{3}$ arrangement predominates.[10] The unit cell parameter of the 4 × 4 structure was measured to be 11.78 Å and incorporated three hexagonal unit cells of silicene with a unit cell parameter of 3.926 Å; this value being just 1.2% larger than that calculated here, suggesting the presence of a small amount of tensile

strain. However, the interaction with the silver substrate is complicated with substrate induced symmetry breaking, resulting in 2/3 of the atoms being closer to the surface due to strong Si (3p) and Ag (5d) hybridization. For silicene and germanene in the high buckling form, the changes in the band structure make it increasingly difficult to distinguish which bands are crossing one another. In the high buckling configuration, the significant movement of the atoms away

from planarity allows the spin−orbit interaction to induce energy gaps. This is noticeable at the K point, where a large energy gap appears in both HB silicene and germanene.

The phonon dispersion curves in Figure 4a,b show that LB silicene and germanene are predicted to be stable with none (in silicene) and only a small extent (germanene) of the phonons having negative frequencies. As summarized in Table 1, the frequency of the zone center phonon in the LB configuration of silicene and germanene is 556 and 292 cm^{-1}, respectively. This value is lower than the corresponding mode in the planar monolayer (being 604 and 336 cm^{-1}, respectively); the reduction in the phonon frequency is attributed to the longer bond length. Scalise et al. reported similar vibrational modes at 575 cm^{-1} (silicene) and 285 cm^{-1} (germanene), though the exact value depends on the choice of exchange-correlation functional employed in their calculations.[27] Our calculations show that in the low buckling configuration, the defect-activated Raman D peak appears at 503 cm^{-1} (silicene) and 274 cm^{-1} (germanene), respectively. The separation in frequency between the G and D peaks is far smaller than in graphene and a notable feature of the experimental Raman signal is an asymmetry broadening of the line shape. For example, Cinquanta et al.,[10] in their study of silicene containing the 4 × 4 and $\sqrt{13} \times \sqrt{13}$ superstructures, found an asymmetry line shape at 516 cm^{-1} accompanied by broad shoulder extending down to about 440 cm^{-1}. The reason for the broadening is a combination of Raman peaks arising from the different atomic configurations. Lu et al. also reported a low frequency Raman mode at 506 cm^{-1} from a 3.5 nm thick crystalline nanosheet with 400 nm diameter. The full-width half-maximum of the Raman band was 30 cm^{-1}, which is larger than that found in bulk crystalline Si (20 cm^{-1}).[30]

For the HB configurations (Figure 4c,d), substantial negative frequencies across much of the Brillouin zone can be seen and this contributes to ML instability. Here there are distinct differences in the order of the phonon modes between planar or LB silicene and germanene. In the HB configuration at the Γ point, the highest optical branch is now the ZO mode (at 392 cm^{-1} in silicene and 195 cm^{-1} in germanene) and it is predicted to be Raman active. For silicene, the TO and LO modes are predicted to have positive frequencies but, in germanene, they are negative. At the K point in germanene, it is the TO vibrational mode that is calculated to have a substantially negative frequency; this implies that it is the in-plane vibrations that are causing high buckling germanene ML to be unstable. These TO and LO vibrations stretch the bond lengths of the highly buckled sheet, moving the atoms into a geometry that would result in germanene breaking-up into islands or nanoribbons.

5. ELECTRON−PHONON COUPLING AND CARRIER RELAXATION IN SILICENE AND GERMANENE

Calculation and proper identification of the phonon dispersion has important consequences for the treatment of transport and carrier relaxation. Previously, it has been reported[20] that the use of the Born−Opppenheimer approximation was not valid in the study of graphene, as the inverse of the frequency of the zone center E$_{2g}$ vibrational mode was very much shorter than the momentum relaxation time of the electrons. Shao et al. have recently calculated τ_R at 300 K near the Dirac point for silicene to be 1.8 ps for both electrons and holes;[21] no values are known for germanene. The inverse frequency of the high frequency mode at the Γ vibrational mode is calculated here to be 10 fs

for LB silicene and 18 fs for LB germanene, so it can be expected that problems with trying to apply the Born-Oppenheimer approximation to understand carrier relaxation in silicene and germanene will also emerge. An alternative carrier relaxation route that does not involve zone center optical phonons is via coupling to phonons at other high symmetry points. For example, carrier relaxation in graphene can be achieved by coupling of electrons to zone boundary (K point) momentum phonons,[31] hence estimates of electron−phonon coupling strength at the high symmetry points are important. Optical phonon emission occurs when the carrier has exceeded the threshold phonon energy.[19] For graphene, we calculate that this will occur via emission of a zone center phonon with an energy of 194 meV and a zone boundary phonon of 166 meV. For the stable form of silicene, the highest phonon energies are calculated to be 69 and 62 meV, respectively, and for germanene, they are 36−34 meV. As we shall show below, an important difference between silicene and germanene when compared to graphene is the estimation of the efficiency of this alternative relaxation route, even though the threshold energies for phonon emission in silicene and germanene are lower than in graphene.

Electron−phonon coupling can be defined as the derivative of the hopping integral with respect to the carbon bond distance. The strength of the coupling can be described[31,32] in terms of the EPC matrix element, $D_{(k+q)n,km}$, given by

$$D_{(k+q)n,km} = \langle k+q, n|\Delta V_q[\Delta n_q]|k, m \rangle \tag{1}$$

where ΔV_q and Δn_q are the derivatives of the Kohn−Sham potential and charge density with respect to the displacement along the normal coordinate, respectively, and $|k,n\rangle$ is the electronic Bloch eigenstate at wavenumber k and band n. The EPC can also be expressed in terms of the product of D with the phonon characteristic length to give

$$|g_q|^2 = |D_q|^2 \left(\frac{\hbar}{2M\omega_q} \right) \tag{2}$$

where M is the atomic mass and ω_q is the particular phonon frequency; carrier scattering rates are proportional to g^2. The units of D^2 are eV^2/Å^2 and those of g^2 are eV^2. Equation 2 simplifies to $g_q^2 = 1.402 \times D_q^2/\omega_q$ for graphene, $g_q^2 = 0.599 \times D_q^2/\omega_q$ for silicene and $g_q^2 = 0.231 \times D_q^2/\omega_q$ for germanene, with ω measured in cm^{-1} in all three cases. The EPC matrix elements can be calculated[31] from the slope of electronic band structure, β (which is equal to $\hbar v_F$) from Figures 1 and 3 and from the slopes of the phonon dispersion curves from Figures 2 and 4 around the high symmetry Γ and K points via

$$D_q^2 = \frac{8M\omega_q}{\sqrt{3}\,a\hbar} \times \beta \times \frac{d\omega_q}{dK} \tag{3}$$

From Table 1 the valu e of D^2 in graphene is calculated to be 42.6 eV^2/Å^2 for the zone center E$_{2g}$ mode and 65.0 eV^2/Å^2 for the A$_1'$ TO mode at the K point; these values are in good agreement with previous studies.[32] For planar silicene and germanene, the calculated value of D^2 is significantly smaller (1.4 and 0.3 eV^2/Å^2, respectively). For the LB configurations, values of D^2 of 1.9 and 1.6 eV^2/Å^2 are calculated for silicene and germanene, respectively. All these values are about a factor of 25 times smaller than those found in graphene. Examining the form of eq 3 and comparing the relative contributions of the various terms between silicene and graphene shows that the

reduction in the EPC matrix element is primarily associated with the softening of the phonon dispersion curves rather than (i) an increase in atomic mass or lattice constant, (ii) a reduction in phonon frequencies or (iii) decrease in the Fermi velocity. The significantly lower EPC matrix elements in silicene and germanene will result in a lower probability for electrons to relax adiabatically to the ground state through either zone center or zone boundary phonon emission even though the threshold energies for phonon emission are lower.

6. SUMMARY

In conclusion, ab initio calculations of monolayer group IV 2D materials have revealed the presence of linear band dispersion in planar and in low buckling configurations of silicene and germanene with a Fermi velocity that is about two-thirds that found in graphene. Analysis of the phonon dispersion curves shows that the presence of out-of-plane modes in planar silicene and germanene contributes to ML instability. For the high buckled configurations, the presence of significant negative phonon frequencies suggest that free-standing monolayers are unlikely to be stable. Estimates of the electron–phonon coupling matrix elements suggest that the interaction of carriers with phonons is reduced by a factor of about 25 when compared to graphene. This will limit adiabatic relaxation of carriers by coupling to zone center or zone boundary phonons. This will result in long momentum relaxation lengths, high mobilities and will have implications for high field transport studies in group IV monolayer materials.

■ ASSOCIATED CONTENT

Ⓢ Supporting Information

Orbital analysis of the band structure of graphene, planar silicene and planar germanene at the Γ point in the Brillouin zone. This material is available free of charge via the Internet at http://pubs.acs.org.

■ AUTHOR INFORMATION

Corresponding Authors

*N.J.R. E-mail: N.Roome@surrey.ac.uk.
*J.D.C. E-mail: David.Carey@surrey.ac.uk.

Notes

The authors declare no competing financial interest.

■ ACKNOWLEDGMENTS

■ REFERENCES

(1) Geim, A. K.; Grigorieva, I. V. van der Waals Heterostructures. *Nature* **2013**, *499*, 419−425.

(2) Novoselov, K. S.; Geim, A. K.; Morozov, S. V.; Jiang, D.; Zhang, Y.; Dubonos, S. V.; Grigorieva, I. V.; Firsov, A. A. Electric Field Effect in Atomically Thin Carbon Films. *Science* **2004**, *306*, 666−669.

(3) Dean, C. R.; Young, A. F.; Meric, I.; Lee, C.; Wang, L.; Sorgenfrei, S.; Watanabe, K.; Taniguchi, T.; Kim, P.; Shepard, K. L.; et al. Boron Nitride Substrates for High-Quality Graphene Electronics. *Nat. Nanotechnol.* **2010**, *5*, 722−726.

(4) Mak, K. F.; Lee, C.; Hone, J.; Shan, J.; Heinz, T. F. Atomically Thin MoS$_2$: A New Direct-Gap Semiconductor. *Phys. Rev. Lett.* **2010**, *105*, 136805.

(5) Novoselov, K. S.; Geim, A. K.; Morozov, S. V.; Jiang, D.; Katsnelson, M. I.; Grigorieva, I. V.; Dubonos, S. V.; Firsov, A. A. Two-

Dimensional Gas of Massless Dirac Fermions in Graphene. *Nature* **2005**, *438*, 197−200.

(6) Tzalenchuk, A.; Lara-Avila, S.; Kalaboukhov, A.; Paolillo, S.; Syväjärvi, M.; Yakimova, R.; Kazakova, O.; Janssen, T. J. B. M.; Fal'ko, V. I.; Kubatkin, S. Towards a Quantum Resistance Standard Based on Epitaxial Graphene. *Nat. Nanotechnol.* **2010**, *5*, 186−189.

(7) Wang, X.; Zhi, L.; Mullen, K. Transparent Conductive Graphene Electrodes for Dye-Sensitized Solar Cells. *Nano Lett.* **2008**, *8*, 323−327.

(8) Lin, Y. M.; Dimitrakopoulos, C.; Jenkins, K. A.; Farmer, D. B.; Chiu, H. Y.; Grill, A.; Avouris, P. 100 GHz Transistors from Wafer-scale Epitaxial Graphene. *Science* **2010**, *327*, 662.

(9) Vogt, P.; De Padova, P.; Quaresima, C.; Avila, J.; Frantzeskakis, E.; Asensio, M. C.; Resta, A.; Ealet, B.; Le Lay, G. Silicene: Compelling Experimental Evidence for Graphenelike Two-Dimensional Silicon. *Phys. Rev. Lett.* **2012**, *108*, 155501.

(10) Cinquanta, E.; Scalise, E.; Chiappe, D.; Grazianetti, C.; van den Broek, B.; Houssa, M.; Fanciulli, M.; Molle, A. Getting through the Nature of Silicene: An sp^2-sp^3 Two-Dimensional Silicon Nanosheet. *J. Phys. Chem. C* **2013**, *117*, 16719−16724.

(11) Meng, L.; Wang, Y.; Zhang, L.; Du, S.; Wu, R.; Li, L.; Zhang, Y.; Li, G.; Zhou, H.; Hofer, W. A.; et al. Buckled Silicene Formation on Ir(111). *Nano Lett.* **2013**, *13*, 685−690.

(12) De Padova, P.; Kubo, O.; Olivieri, B.; Quaresima, C.; Nakayama, T.; Aono, M.; Le Lay, G. Multilayer Silicene Nanoribbons. *Nano Lett.* **2012**, *12*, 5500−5503.

(13) Fleurence, A.; Friedlein, R.; Ozaki, T.; Kawai, H.; Wang, Y.; Yamada-Takamura, Y. Experimental Evidence for Epitaxial Silicene on Diboride Thin Films. *Phys. Rev. Lett.* **2012**, *108*, 245501.

(14) Restrepo, O. D.; Mishra, R.; Goldberger, J. E.; Windl, W. Tunable Gaps and Enhanced Mobilities in Strain-Engineered Silicane. *J. Appl. Phys.* **2014**, *115*, 033711.

(15) Bianco, E.; Butler, S.; Jiang, S.; Restrepo, O. D.; Windl, W.; Goldberger, J. E. Stability and Exfoliation of Germanane: A Germanium Graphane Analogue. *ACS Nano* **2013**, *7*, 4414−4421.

(16) Kaloni, T. P.; Schwingenschlögl, U. Epitaxial Growth of Germanene on a GaAs (0001) Substrate: A First Principles Approach. *J. Appl. Phys.* **2013**, *114*, 184307.

(17) Xu, Y.; Yan, B.; Zhang, H.-J.; Wang, J.; Xu, G.; Tang, P.; Duan, W.; Zhang, S.-C. Large-Gap Quantum Spin Hall Insulators in Tin Films. *Phys. Rev. Lett.* **2013**, *111*, 136804.

(18) Cahangirov, S.; Topsakal, M.; Akturk, E.; Şahin, H.; Ciraci, S. Two- and One-Dimensional Honeycomb Structures of Silicon and Germanium. *Phys. Rev. Lett.* **2009**, *102*, 236804.

(19) Dorgan, V. E.; Behnam, A.; Conley, H. J.; Bolotin, K. I.; Pop, E. High-Field Electrical and Thermal Transport in Suspended Graphene. *Nano Lett.* **2013**, *13*, 4581−4586.

(20) Pisana, S.; Lazzeri, M.; Casiraghi, C.; Novoselov, K. S.; Geim, A. K.; Ferrari, A. C.; Mauri, F. Breakdown of the Adiabatic Born-Oppenheimer Approximation in Graphene. *Nat. Mater.* **2007**, *6*, 198−201.

(21) Shao, Z.-G.; Ye, X.-S.; Yang, L.; Wang, C.-L. First-principles Calculation of Intrinsic Carrier Mobility of Silicene. *J. Appl. Phys.* **2013**, *114*, 093712.

(22) Hammer, B.; Hansen, L. B.; Nørskov, J. K. Improved Adsorption Energetics Within Density Functional Theory Using Revised Perdew-Burke-Ernzerhof Functionals. *Phys. Rev. B* **1999**, *59*, 7413−7421.

(23) Delley, B. From Molecules to Solids with the DMol^3 Approach. *J. Chem. Phys.* **2000**, *113*, 7756−7764.

(24) Segall, M. D.; Lindan, P. J. D.; Probert, M. J.; Pickard, C. J.; Hasnip, P. J.; Clark, S. J.; Payne, M. C. First-principles Simulation: Ideas, Illustrations and the CASTEP code. *J. Phys.: Condens. Matter* **2002**, *14*, 2717−2744.

(25) Baroni, S.; de Gironcoli, S.; Dal Corso, A.; Giannozzi, P. Phonons and Related Properties of Extended Systems from Density Functional Perturbation Theory. *Rev. Mod. Phys.* **2001**, *73*, 515−562.

7749

dx.doi.org/10.1021/am501022x | *ACS Appl. Mater. Interfaces* 2014, 6, 7743−7750

(26) Houssa, M.; Pourtois, G.; Afanas'ev, V. V.; Stesmans, A. Electronic Properties of Two-Dimensional Hexagonal Germanium. *Appl. Phys. Lett.* **2010**, *96*, 082111.

(27) Scalise, E.; Houssa, M.; Pourtois, G.; van den Broek, B.; Afanas'ev, V.; Stesmans, A. Vibrational Properties of Silicene and Germanene. *Nano Res.* **2013**, *6*, 19−28.

(28) Guzmán-Verri, G. G.; Lew Yan Voon, L. C. Electronic Structure of Silicon-based Nanostructures. *Phys. Rev. B* **2007**, *76*, 075131.

(29) Khan, R. U. A.; Carey, J. D.; Silva, S. R. P.; Jones, B. J.; Barklie, R. C. Electron Delocalization in Amorphous Carbon by Ion Implantation. *Phys. Rev. B* **2001**, *63*, 121201.

(30) Lu, Z.; Zhu, J.; Sim, D.; Zhou, W.; Shi, W.; Hng, H. H.; Yan, Q. Synthesis of Ultrathin Silicon Nanosheets by using Graphene Oxide as Template. *Chem. Mater.* **2011**, *23*, 5293−5295.

(31) Lazzeri, M.; Piscanec, S.; Mauri, F.; Ferrari, A. C.; Robertson, J. Electron Transport and Hot Phonons in Carbon Nanotubes. *Phys. Rev. Lett.* **2005**, *95*, 236802.

(32) Piscanec, S.; Lazzeri, M.; Robertson, J.; Ferrari, A. C.; Mauri, F. Optical Phonons in Carbon Nanotubes: Kohn Anomalies, Peierls Distortions and Dynamic Effects. *Phys. Rev. B* **2007**, *75*, 035427.